



Non-Gaussian data assimilation of satellite-based Leaf Area Index observations with an individual-based dynamic global vegetation model

Hazuki Arakida¹, Takemasa Miyoshi^{1,2,3}, Takeshi Ise⁴, Shin-ichiro Shima^{1,5}, and Shunji Kotsuki¹

5 ¹RIKEN Advanced Institute for Computational Science, Kobe, 650-0047, Japan

²Department of Atmospheric and Oceanic Science, University of Maryland, College Park, MD 20742, USA

³Application Laboratory, Japan Agency for Marine-Earth Science and Technology, Yokohama, 236-0001, Japan

⁴Field Science Education and Research Center, Kyoto University, Kyoto, 606-8502, Japan

⁵Graduate School of Simulation Studies, University of Hyogo, Kobe, 650-0047, Japan

10 *Correspondence to:* Hazuki Arakida (hazuki.arakida@riken.jp) and Takemasa Miyoshi (takemasa.miyoshi@riken.jp)

Abstract. We newly developed a data assimilation system based on a particle filter approach with the Spatially Explicit Individual-Based Dynamic Global Vegetation Model (SEIB-DGVM). We first performed an idealized observing system simulation experiment to evaluate the impact of assimilating the leaf area index (LAI) data every 4 days, assuming the satellite-based LAI. Although we assimilated only LAI as a whole, the forest and grass LAIs were estimated separately with high accuracy. Uncertain model parameters and other state variables were also estimated accurately. Therefore, we extended the experiment to the real world using the real Moderate Resolution Imaging Spectroradiometer (MODIS) LAI data, and obtained promising results.

1 Introduction

The terrestrial biosphere is an important part of the Earth System Model (ESM) to simulate the carbon and water cycles. However, terrestrial biosphere models tend to have large uncertainties, for example, in phenology (Richardson et al., 2012; Murray-Tortarolo et al., 2013) and in spatial distributions of plant species (Cheaib et al., 2012). Recently, data assimilation (DA) methods which incorporate observation data into models have been applied to terrestrial biosphere models to reduce the uncertainties in the state variables and model parameters (Luo et al., 2011; Peng et al., 2011). Previous studies have successfully applied the ensemble Kalman filter (e.g., Evensen, 2003; Williams et al., 2005; Quaife et al., 2008; Stöckli et al., 2011) or adjoint method (e.g., Kaminski et al., 2013; Kato et al., 2013) to the *static* vegetation models, but studies with the *dynamic* global vegetation models (DGVMs) are still limited (Luo et al., 2011; Peng et al., 2011), although Hartig et al. (2012) pointed out the importance.

The *static* vegetation models are time-independent and do not include the vegetation succession process (Peng, 2000). Alternatively, DGVMs include the vegetation succession process and can simulate carbon and water cycle changes linking to the vegetation shift under the changing climate. Especially, *individual-based* DGVMs simulate local interactions among individual plants such as competitions for light and water, so that the model can simulate the vegetation succession more explicitly (Smith et al., 2001; Sato et al. 2007). Garetta et al. (2010) pioneered to apply DA to an *individual-based* DGVM



for paleoclimate, but no study has been published thus far to assimilate fine time-scale data from satellites and ground stations using an *individual-based* DGVM. If the initial vegetation structure and the model parameters of an *individual-based* DGVM are estimated more accurately by assimilating the fine time-scale data, the uncertainties of the simulated future vegetation would be greatly reduced.

5 This study explores to assimilate frequent satellite-based Leaf Area Index (LAI) data with an *individual-based* DGVM known as the SEIB-DGVM, standing for Spatially Explicit Individual-Based DGVM (Sato et al., 2007). We newly developed a non-Gaussian ensemble DA system with the SEIB-DGVM based on a particle filter approach. As the first step, this study performs a series of numerical experiments at a local scale. It would be straightforward to extend it to the global scale, since the local-scale experiments can be performed in parallel for different locations. In this study, we first perform an
10 idealized experiment to investigate how well we can estimate the model parameters associated with phenology by assimilating the LAI data every 4 days, assuming the satellite-based LAI product from the Moderate Resolution Imaging Spectroradiometer (MODIS) aboard the Terra and Aqua spacecraft. We also investigate to what extent assimilating the LAI data could improve the estimates of the state variables such as GPP (Gross Primary Production), RE (Ecosystem Respiration), NEE (Net Ecosystem Exchange), and biomass, the most fundamental variables for carbon cycle and vegetation states.
15 Following the idealized experiment, we perform an experiment using the real MODIS LAI observation data to see how the proposed approach works in the real world.

2 Methods

2.1 SEIB-DGVM

The SEIB-DGVM simulates establishment, growth, and decay of the individuals of prescribed plant functional types
20 (PFTs) within a spatially explicit virtual forest (Sato et al., 2007), forced by climate conditions such as air temperature, soil temperature, cloudiness, precipitation, humidity, and winds. We used version 2.71 (Sato and Ise, 2012) but with minimal modifications for DA (cf. Appendix). Among the various model outputs ranging from individual tree height to soil water content (Sato et al., 2007, with updated information available from the package of version 2.71), we focus on LAI because it is a key to the vegetation model, and because previous studies show a promise in assimilating satellite-based LAI data with a
25 *static* vegetation model (Stöckli et al., 2011) and a *non-individual-based* DGVM (Demarty et al., 2007). We extend the previous studies to assimilate the LAI data with the *individual-based* DGVM.

2.2 Particle filter-based DA

Individual-based DGVMs include highly nonlinear processes such as occasional establishment and death of individual plants. These processes produce and eliminate state variables, and the phase space changes time to time. DA methods that
30 have been used in geophysical applications usually assume that the state variables are defined uniquely for the given dynamical system and that the phase space stays the same. The widely-used ensemble Kalman filter, for example, finds the



best linear combination of the ensemble with optimal fit to the observations, but it is not trivial to define a linear combination or even the ensemble mean for the variables missing in some ensemble members. Therefore, it would not be trivial to apply the widely-used DA methods to *individual-based* DGVMs.

Alternatively, particle filters run independent parallel simulations or particles and represent the probability density function (PDF) explicitly by assigning probability to each particle. Therefore, particle filters can handle non-Gaussianity and nonlinearity explicitly, and can be applied to the *individual-based* DGVMs in a straightforward manner (e.g., Garetta et al., 2010) even though the phase space is different for each particle.

Here we adopt an efficient particle filter approach known as the Sequential Importance Resampling (SIR: Fig. 1) (Gordon et al., 1993). First, n parallel simulations are performed, and each simulation is considered as a particle representing the true state of the system with equal probability. Next, likelihood $l_t^{(i)}$ is calculated for each particle using the Gaussian likelihood function:

$$l_t^{(i)} = p(y_t | x_{t|t-1}^{(i)}) = \frac{1}{\sqrt{2\pi} \cdot \sigma^2} \exp \left\{ -\frac{(y_t - x_{t|t-1}^{(i)})^2}{2 \cdot \sigma^2} \right\} \quad \text{for } i = 1, \dots, n.$$

Here, $x_{t|t-1}^{(i)}$ denotes the simulated LAI of the i th particle at time t from the previous time step $t-1$, y_t the observed LAI at time t , and σ the observation error standard deviation. Since the prior probability is uniform, Bayes' rule gives that the posterior probability of the i th particle is proportional to $l_t^{(i)}$, i.e., the particles closer to the observation have more probability. Next, we resample the particles, so that each particle has equal probability. The particles with more probability (larger $l_t^{(i)}$) are duplicated, and the particles with less probability (smaller $l_t^{(i)}$) are removed. If n is sufficiently large, we can evaluate the posterior PDF accurately. Each resampled particle represents the true state of the system with equal probability and acts as the initial particle for the next time step. This Bayesian framework is repeated.

2.3 OSSE and the real-world experiment

We first perform an idealized Observing System Simulation Experiment (OSSE). The OSSE (e.g., Atlas, 1997) is a widely-used approach in meteorological DA to test the general performance of a DA system and to evaluate the impact of specific observing systems. OSSE has the nature run, which is usually generated by running a simulation for a certain period. Observation data are simulated from the nature run by applying the observation operator, i.e., converting the model variables to the observed variables. Here, we add artificial random noise to simulate the observation error. DA experiments are initiated from the state independent of the nature run, and the simulated observations are assimilated. The resulting analyses and subsequent forecasts are compared with the nature run to evaluate the performance of DA. Once an OSSE is done, it is straightforward to extend the OSSE to the real world by simply replacing the simulated observations with the real-world observations.



3 OSSE

3.1 Experimental design

To generate the nature run, the SEIB-DGVM was initialized with the bare ground (i.e., no plant at the beginning) and was run for 107 years using the climate forcing data from year 2001 to 2010 available at the SEIB-DGVM webpage (<http://seib-dgvm.com/>). Here, the 10-year forcing data are repeated for the 107-year simulation, and the last 7 years from year 101 to 107 use the actual climate forcing of 2001 to 2007, so that we call year 101 to 107 to be 2001 to 2007. The daily climate data were generated by the procedure of Sato and Ise (2012) with updated information available at the SEIB-DGVM webpage, based on the monthly Climate Research Unit observation-based data (CRU-TS3.22 0.5-degree monthly climate time series) (Harris et al., 2014) and the daily data from the National Centers for Environmental Prediction (NCEP)/National Center for Atmospheric Research (NCAR) reanalysis (Kalnay et al., 1996). We chose the study area at one of the AsiaFlux sites, the Siberia Yakutsk Larch forest site at Spasskaya Pad, the middle basin of River Lena (62° 15' 18" N, 129° 14' 29" E). Field observation data are available as the ground truth to verify the DA results at this site. Forced by the climate data, the SEIB-DGVM simulates the vegetation shifts from the bare ground to a grassland, and then to a forest. The two PFTs, the boreal deciduous needle leaved trees and C3 grass, are the dominant PFTs in this study area. Therefore, we do not consider the other PFTs in this study. We call these two PFTs simply “forest” and “grass”.

The nature run (Fig. 2 a) was performed with the “true” parameter values $P_{\max} = 15 \mu\text{molCO}_2 \text{ m}^{-2} \text{ s}^{-1}$ and $D_{\text{or}} = 230$ DOY (day of year) for forest and $P_{\max} = 9 \mu\text{molCO}_2 \text{ m}^{-2} \text{ s}^{-1}$ and $D_{\text{or}} = 270$ DOY for grass, where P_{\max} and D_{or} stand for the maximum photosynthesis rate and the start date of the dormancy, respectively (Fig. 2 b). Hereafter we omit the units for P_{\max} ($\mu\text{molCO}_2 \text{ m}^{-2} \text{ s}^{-1}$) and D_{or} (DOY) for simplicity. The LAI observations for the last 4 years from year 2004 to 2007 were created by adding independent Gaussian random noise to the LAI values from the nature run (Fig. 2 a) every 4 days, assuming the MODIS LAI product. Here, the observation error standard deviation was given by 10 % of the nature run LAI value. The observed LAI < 0.5 are discarded and not used for DA.

Next, 8000 particles (parallel simulations) were generated with uniformly perturbed parameters: $P_{\max} = [0, 60]$ for forest, $P_{\max} = [0, 15]$ for grass, $D_{\text{or}} = [200, 300]$ for both. Here, $[a, b]$ denotes random draws from the uniform distribution between a and b . We ran 8000 parallel simulations for 103 years for spin-up from the bare ground using the same climate forcing data as the nature run. In the course of the vegetation succession, these randomly perturbed parameter sets result in a variety of LAI simulations (Fig. 2 b).

The 8000 particles at the end of the 103-year spin-up runs are used as the initial conditions for DA. The simulated LAI observations are assimilated every 4 days. The nature run and particle filter use the same climate forcing data, so that the difference comes from the model parameter values. To avoid the exact duplications and convergence after resampling, the model parameters P_{\max} and D_{or} are randomly perturbed for the duplicated particles. Here, random draws $[-4, 4]$ are added to P_{\max} for forest and to D_{or} for both forest and grass, and $[-1, 1]$ is added to P_{\max} for grass. In case that these perturbed parameters exceed the corresponding initial parameter range, the excess value was bounced back from the limits. To assess



the impact of DA, we also perform an experiment without DA (“NODA” hereafter), and compare to the experiment with DA (“TEST” hereafter).

3.2 Results

Figure 3 shows the time series of LAI for NODA (left) and TEST (right). The observations (Fig. 3 a, red dots with error bars) cannot distinguish the forest and grass, but the model simulates LAIs for forest and grass separately (Fig. 3 b, c). Although the particles without DA are widely spread (left, gray areas), DA makes the particles much narrower (right) and consistent with the nature run (red curves). With DA, the median of the particles for forest is almost identical to the nature run for the entire 4 years (Fig. 3 b, right). As for grass, the median of the particles is also very close to the nature run with DA, but in the first three years the dormancy period is delayed (Fig. 3 c, right).

The model parameters are estimated accurately (Fig. 4). There is no direct observation of these parameters, so that the estimations are purely due to DA of the LAI observations. Although the particles of the NODA experiment are uniformly distributed (Fig. 4, left), DA makes the particles close to the true parameters (Fig. 4, right). It takes 1-4 years until the true values fall within the quartiles of the particles. The Pmax estimates for both forest and grass show occasional jumps, but tend to stay around the true values (Fig. 4 a, b). Dor for forest seems the most accurate and stable after the dormancy period of the first year (Fig. 4 c). Dor for grass takes the longest; the estimation is not accurate until the dormancy of the fourth year (Fig. 4 d). This may be related to the previous results showing the erroneous estimates of the grass LAI near the dormancy period in the first 3 years (Fig. 3 c).

Other model variables such as GPP, RE, NEE and biomass show large improvements (Fig. 5). Although the particles of the NODA experiment are widely spread, DA with only LAI observations greatly reduces the uncertainties for the four variables, and the estimations are generally reasonable.

To investigate the sensitivity to the choice of the nature run, we performed similar OSSEs by replacing the nature run with other randomly-chosen parameter sets. Also, we generated different random numbers for the observation errors. The results showed similar results with the different nature runs and random numbers.

4 Real-world experiment

4.1 Experimental settings

The OSSE was extended to the real world by replacing the simulated observations with the real observations. Since the OSSE used the actual climate forcing in 2004 to 2007, we used the quality controlled MODIS LAI product of MCD15A3 for those years with flagged as “good quality”, “Terra or Aqua”, “detectors apparently fine for up to 50 %”, “significant clouds not present”, and “main method used with or without saturation”. We took the median of the LAI observations in the 10-km radius from the study site (62° 15' 18" N, 129° 14' 29" E). The gridded MODIS LAI data have the grid resolution of 1 km, so that the 10-km radius area contains 314 grid points. If more than 14 grids are missing, we apply missing data for DA. The



observation error standard deviations are assigned to each LAI datum from the original source, and we took the median of the error standard deviations.

The model-simulated NEE was validated with the field observation data at this AsiaFlux site (Ohta et al., 2001; 2008; 2014). The data was quality controlled by the steady-state test as indicated by the quality flag 0. Although the model
5 simulates daily-average NEE, the field observation data represent instantaneous NEE every 30 minutes. The observation data are missing frequently, and it is not trivial to derive daily averages. Therefore, the raw data are compared with the DA results directly. This allows only a rough verification about whether or not the simulated NEE is in a reasonable range, but this is the only possible verification with an independent source.

10 4.2 Results

Figures 6, 7, and 8 show similar time series to Figs. 3, 4, and 5, respectively, but with the real MODIS LAI observations. Although the particles of the NODA experiments are widely spread, DA makes the particles much narrower (right) for all variables and parameters. With DA, the median of LAI is very close to the observations, within the range of the observation error standard deviations (Fig. 6 a). The grass and forest LAIs are estimated separately (Fig. 6 b, c), but there is no direct
15 observation or other verification truth to compare with. This is similar to the model parameters (Fig. 7) and other model variables (Fig. 8) except for NEE, for which direct field observation data are available. As in the OSSE results, the range of uncertainties for NEE is reduced significantly by DA (Fig. 8 c). Since the field observations are made instantaneously every 30 minutes, the observation values (red) appear to have a wider range. However, the SEIB-DGVM simulates only daily-average NEE, and it is not straightforward to compare the outputs from SEIB-DGVM with the field observations. We still
20 find that the median of NEE becomes closer to the observations, particularly near the dormancy period. The simulated NEE generally stays within the reasonable range compared with the field observations. In general, the particle filter shows promising results with the real MODIS LAI data.

5 Conclusion

25 We assimilated the satellite-based MODIS LAI data using a non-Gaussian ensemble DA system with the SEIB-DGVM based on the SIR particle filter approach. To the best of the authors' knowledge, this is the first study to assimilate the fine time-scale satellite data with an *individual-based* DGVM. We found that the newly developed DA system greatly reduced the uncertainties of the state variables and model parameters.

Although we assimilated only LAI as a whole, the forest and grass LAIs were estimated separately. This suggests that the
30 satellite-based DA reduce the uncertainties in the initial vegetation structure of the *individual-based* DGVM toward the simulation of the future vegetation change. Another notable results include that the model parameters of the *individual-based*



DGVM were estimated successfully, and that the uncertainties in the unobserved model variables relevant to carbon cycle and vegetation states were also reduced significantly. Similarly to the previous studies with a *static* vegetation model (Stöckli et al., 2011) and a *non-individual-based* DGVM (Demarty et al., 2007), the results in the present study also suggest that LAI be the key to DA for phenology and carbon dynamics.

- 5 As the first step, this study estimated only four parameters using LAI observations at a single location. As a next step, more parameters should be considered at different locations. Local-scale experiments can be performed in parallel for different locations since the satellite-based LAI observations are available globally. The simulation with the initial states and parameter sets obtained from the SEIB-DGVM-based DA system would be expected to improve the estimates of the carbon cycle changes at the global domain.

10



Appendix: List of modifications to SEIB-DGVM ver.2.71.

Parameter modifications	
ce water (no dimension, the minimum value): limitation on photosynthesis via soil water	from 0.001999 to 0.19
Days leaf shed (days): day length required for full leaf drop	from 14 to 30
Days release larch (days): days required for full release of stock energy for larch	from 7 to 60
Delay from foliation (days): delay of stem growth and reproduction process after foliation	from 21 to 0
TO r (times / year): turn over time for root (Forest). We set the same value as the other boreal forest PFTs.	from 0.16 to 0.42
Tmin (°C): minimum temperature (Forest). We set the same value as the other boreal forest PFTs.	from 5.0 to -4.0
Est scenario: Scenario for establishment for forest. Only specified woody PFT was set to establish.	-
Est pft OnOff: Establish switch for forest. Only boreal deciduous needle leaved tree was set to establish.	-
Parameter modifications (H. Sato, personal communication, 2014)	
TO f (times / year): turn over time for foliage (Grass)	from 0.50 to 3.19
ALM1 (m ² / m): Allometry index of LA vs dbh of sapwood (Forest)	from 6000 to 0
ALM3 (g dm / m ³): Allometry index of trunk mass (Forest)	from 0 to 700000
FR_ratio (g dm / g dm): ratio of leaf mass vs root mass (Forest)	from 0.17 to 0.35
FR_ratio (g dm / g dm): ratio of leaf mass vs root mass (Grass)	from 0.33 to 0.10
SLA (one sided m ² / g dm): specific leaf area (Forest)	from 0.014 to 0.010
SLA (one sided m ² / g dm): specific leaf area (Grass)	from 0.015 to 0.020
Topt0 (°C): optimum temperature (Forest)	from 20.0 to 21.0
Tmax (°C): maximum temperature (Forest)	from 35.0 to 38.0
GS_b2 (no dimension): parameters of stomatal conductance (Grass)	from 3.0 to 5.0
M1 (no dimension): asymptotic maximum mortality rate (Forest)	from 0.003 to 0.001
TC_min (°C): minimum coldest month temperature for persisting (Forest and Grass)	from -1000.0 to -45.0
GDD_min (5 °C base): minimum degree-day sum for establishment (Forest)	from 350 to 250
Model modifications	
Foliage: If cumulative air temperature greater than 4.1°C >= 65 °C, leaves of forest start opening. If 7days cumulative optimum LAI for grass > 0.01, leaves of grass start opening. → If the day of the year >=110, leaves of forest and grass start opening.	
Dormancy: If 10 days running mean of air temperature < 7 °C, leaves of forest start falling. If 7 days cumulative optimum LAI for grass <= 0.01, leaves of grass start falling. → If the day of the year >= Dor for forest or >= Dor for grass, leaves start falling. If the day from leaf onset <60, the phenology can't change from foliage to dormancy. → This if statement was deleted.	
Fire function was excluded.	
Bug fix: Gradual release of stock energy If day from leaf onset >= day length for full release of stock, stock energy is released. → If day from leaf onset >= (day length for full release of stock - 1), stock energy is released.	
Bug fix: Maintenance respiration (Herbaceous PFTs, source1) If resource required for maintenance respiration < available biomass of grass, biomass for combust = biomass for combust + resource required for maintenance respiration → biomass for combust = biomass for combust + resource required for maintenance respiration * x (if the PFT foliates, x=1, else x=0.1) NPP of the PFT= NPP of the PFT – resource required for maintenance respiration →NPP of the PFT= NPP of the PFT – resource required for maintenance respiration * x (if the PFT foliates, x=1, else x=0.1)	



Acknowledgements

The authors thank Hisashi Sato, the main developer of SEIB-DGVM, for useful discussions. The source code of SEIB-DGVM and the climate forcing data are available at <http://seib-dgvm.com/>. MODIS LAI product of MCD15A3 was retrieved from the online Data Pool, courtesy of the NASA Land Processes Distributed Active Archive Center (LP DAAC),
5 USGS/Earth Resources Observation and Science (EROS) Center, Sioux Falls, South Dakota
(https://lpdaac.usgs.gov/data_access/data_pool). Carbon flux data was retrieved from AsiaFlux database
(<https://db.cger.nies.go.jp/asiafluxdb/>).

References

- Atlas, R.: Atmospheric observations and experiments to assess their usefulness in data assimilation, *J. Meteorol. Soc. Jpn.*,
10 75, 111–130, 1997.
- Cheaub, A., Badeau, V., Boe, J., Chuine, I., Delire, C., Dufrière, E., François, C., Gritti, E. S., Legay, M., Pagé, C., Thuiller,
W., Viovy, N., and Leadley, P.: Climate change impacts on tree ranges: model intercomparison facilitates understanding
and quantification of uncertainty, *Ecol. Lett.*, 15, 533–544, 2012.
- Demarty, J., Chevallier, F., Friend, A. D., Viovy, N., Piao, S., and Ciais, P.: Assimilation of global MODIS leaf area index
15 retrievals within a terrestrial biosphere model, *Geophys. Res. Lett.*, 34, L15402, 2007.
- Evensen, G.: The ensemble Kalman filter: Theoretical formulation and practical implementation, *Ocean. Dynam.*, 53, 343-
367, 2003.
- Garreta, V., Miller, P. A., Guiot, J., Hély, C., Brewer, S., Sykes, M. T., and Litt, T.: A method for climate and vegetation
reconstruction through the inversion of a dynamic vegetation model, *Clim. Dynam.*, 35, 371-389, 2010.
- 20 Gordon, N. J., Salmond, D. J., and Smith, A. F. M.: Novel approach to nonlinear/non-Gaussian Bayesian state estimation,
IEE Proc. F, 140, 107-113, 1993.
- Harris, I., Jones, P.D., Osborn, T.J., and Lister, D.H.: Updated high-resolution grids of monthly climatic observations - the
CRU TS3.10 Dataset, *Int. J. Climatol.*, 34, 623-642, 2014.
- Hartig, F., Dyke, J., Hickler, T., Higgins, S. I., O'Hara, R. B., Scheiter, S., and Huth, A.: Connecting dynamic vegetation
25 models to data – an inverse perspective, *J. Biogeogr.*, 39, 2240–2252, 2012.
- Kalnay, E., Kanamitsu, M., Kistler, R., Collins, W., Deaven, D., Gandin, L., Iredell, M., Saha, S., White, G., Woollen, J.,
Zhu, Y., Chelliah, M., Ebisuzaki, W., Higgins, W., Janowiak, J., Mo, K. C., Ropelewski, C., Wang, J., Leetmaa, A.,
Reynolds, R., Jenne, R., and Joseph, D.: The NCEP/NCAR 40-year reanalysis project, *Bull. Amer. Meteor. Soc.*, 77,
437-471, 1996.
- 30 Luo, Y., Ogle, K., Tucker, C., Fei, S., Gao, C., LaDeau, S., Clark, J. S., and Schimel, D. S.: Ecological forecasting and data
assimilation in a data-rich era, *Ecol. Appl.*, 21, 1429–1442, 2011.



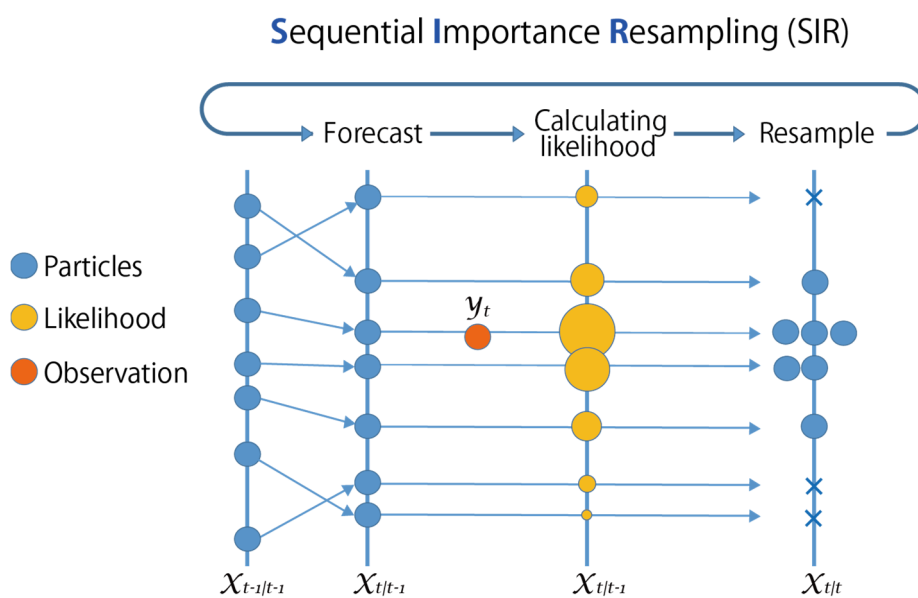
- Kaminski, T., Knorr, W., Schürmann, G., Scholze, M., Rayner, P. J., Zaehle, S., Blessing, S., Dorigo, W., Gayler, V., Giering, R., Gobron, N., Grant, J. P., Heimann, M., Hooker-Stroud, A., Houweling, S., Kato, T., Kattge, J., Kelley, D., Kemp, S., Koffi, E. N., Köstler, C., Mathieu, P. -P., Pinty, B., Reick, C. H., Rödenbeck, C., Schnur, R., Scipal, K., Sebald, C., Stacke, T., Terwisscha van Scheltinga, A., Vossbeck, M., Widmann, H., and Ziehn, T.: The BETHY/JSBACH
5 Carbon Cycle Data Assimilation System: experiences and challenges, *J. Geophys. Res. Biogeosci.*, 118: 1414-1426, 2013.
- Kato, T., Knorr, W., Scholze, M., Veenendaal, E., Kaminski, T., Kattge, J., and Gobron, N.: Simultaneous assimilation of satellite and eddy covariance data for improving terrestrial water and carbon simulations at a semi-arid woodland site in Botswana, *Biogeosciences*, 10, 789-802, 2013.
- Murray-Tortarolo, G., Anav, A., Friedlingstein, P., Sitch, S., Piao, S., Zhu, Z., Poulter, B., Zaehle, S., Ahlström, A., Lomas,
10 M., Levis, S., Viovy, N., and Zeng, N.: Evaluation of land surface models in reproducing satellite-derived LAI over the high-latitude Northern Hemisphere. Part I: Uncoupled DGVMs, *Remote Sens.*, 5, 4819-4838, 2013.
- Ohta, T., Hiyama, T., Tanaka, H., Kuwada, T., Maximov, T.C., Ohata, T., and Fukushima, Y.: Seasonal variation in the energy and water exchanges above and below a larch forest in eastern Siberia, *Hydrol. Process.*, 15, 1459-1476, 2001.
- Ohta, T., Maximov, T. C., Dolman, A. J., Nakai, T., van der Molen, M. K., Kononov, A. V., Maximov, A. P., Hiyama, T.,
15 Iijima, Y., Moors, E. J., Tanaka, H., Toba, T., and Yabuki, H.: Interannual variation of water balance and summer evapotranspiration in an eastern Siberian larch forest over a 7-year period (1998-2006), *Agr. Forest Meteorol.*, 148, 1941-1953, 2008.
- Ohta, T., Kotani, A., Iijima, Y., Maximov, T.C., Ito, S., Hanamura, M., Kononov, A.V., and Maximov, A.P.: Effects of waterlogging on water and carbon dioxide fluxes and environmental variables in a Siberian larch forest, 1998–2011, *Agr. Forest Meteorol.*, 188, 64-75, 2014.
20
- Peng, C.: From static biogeographical model to dynamic global vegetation model: a global perspective on modelling vegetation dynamics, *Ecol. Model.*, 135, 33-54, 2000.
- Peng, C., Guiot, J., Wu, H., Jiang, H., and Luo, Y.: Integrating models with data in ecology and palaeoecology: advances towards a model–data fusion approach, *Ecol. Lett.*, 14, 522–536, 2011.
- 25 Quaife, T., Lewis, P., De Kauwe, M., Williams, M., Law, B. E., Disney, M., and Bowyer, P.: Assimilating canopy reflectance data into an ecosystem model with an Ensemble Kalman Filter, *Remote Sens. Environ.*, 112, 1347-1364, 2008.
- Richardson, A. D., Anderson, R. S., Arain, M. A., Barr, A. G., Bohrer, G., Chen, G., Chen, J. M., Ciais, P., Davis, K. J., Desai, A. R., Dietze, M. C., Dragoni, D., Garrity, S. R., Gough, C. M., Grant, R., Hollinger, D. Y., Margolis, H. A.,
30 McCaughey, H., Migliavacca, M., Monson, R. K., Munger, J. W., Poulter, B., Raczka, B. M., Ricciuto, D. M., Sahoo, A. K., Schaefer, K., Tian, H., Vargas, R., Verbeeck, H., Xiao, J., and Xue, Y.: Terrestrial biosphere models need better representation of vegetation phenology: results from the North American Carbon Program Site Synthesis, *Glob. Change Biol.*, 18, 566–584, 2012.



- Sato, H., Itoh, A., and Kohyama, T.: SEIB–DGVM: A new Dynamic Global Vegetation Model using a spatially explicit individual-based approach, *Ecol. Model.*, 200, 279–307, 2007.
- Sato, H., and Ise, T.: Effect of plant dynamic processes on African vegetation responses to climate change: Analysis using the spatially explicit individual-based dynamic global vegetation model (SEIB-DGVM), *J. Geophys. Res.*, 117, G03017, 5 2012.
- Smith, B., Prentice, I. C., and Sykes, M. T.: Representation of vegetation dynamics in the modelling of terrestrial ecosystems: comparing two contrasting approaches within European climate space, *Global Ecol. Biogeogr.*, 10, 621–637, 2001.
- Stöckli, R., Rutishauser, T., Baker, I., Liniger, M. A., and Denning, A. S.: A global reanalysis of vegetation phenology, *J. Geophys. Res.*, 116, G03020, 2011. 10
- Williams, M., Schwarz, P. A., Law, B. E., Irvine, J., and Kurpius, M. R.: An improved analysis of forest carbon dynamics using data assimilation, *Glob. Change Biol.*, 11, 89–105, 2005.



5



10 **Figure 1.** Schematic showing the SIR particle filter method. The size of the circles corresponds to the assigned probability.



5

10

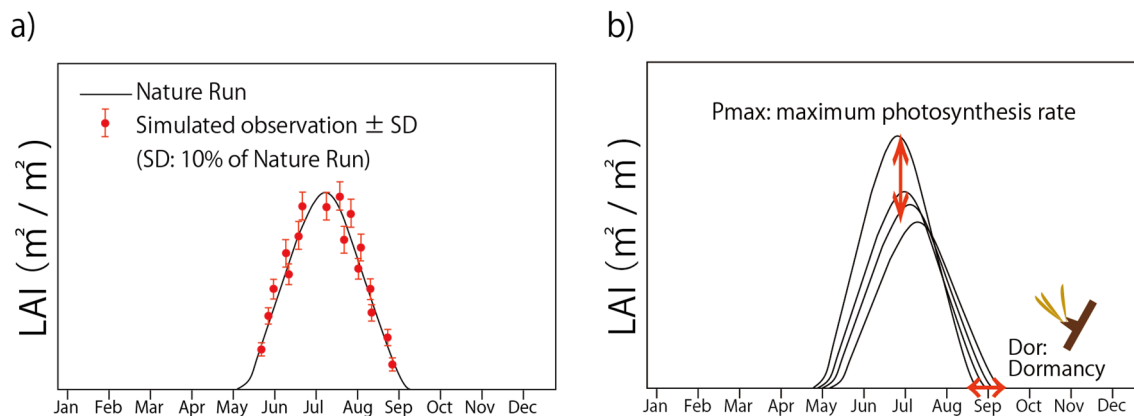


Figure 2. Schematic illustrations of the nature run, observations, and model parameter sensitivities. a) Time series of LAI ($\text{m}^2 \text{m}^{-2}$) for the nature run (black), simulated observations (red dots) and their error standard deviations (SD, red error bars).

15 b) Time series of LAI with different Pmax and Dor values. The perturbed parameters (Pmax and Dor for forest and grass) cause differences between the particles.



5

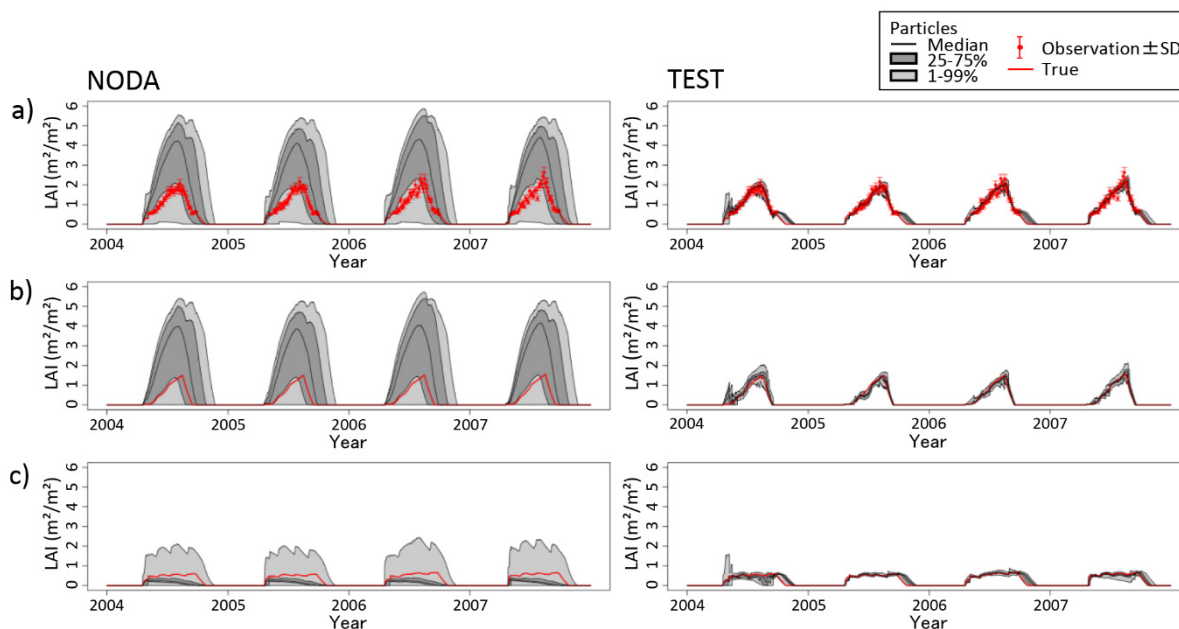


Figure 3. Time series of LAI for a) forest + grass, b) forest, and c) grass for NODA (left) and TEST (right). The dark and light gray areas indicate the quartiles and 1-99 % quantiles of the particles as shown in legend. The thick black curves indicate the medians. The red dots with error bars indicate the observations and their error standard deviations, and the red lines indicate the nature run.



5

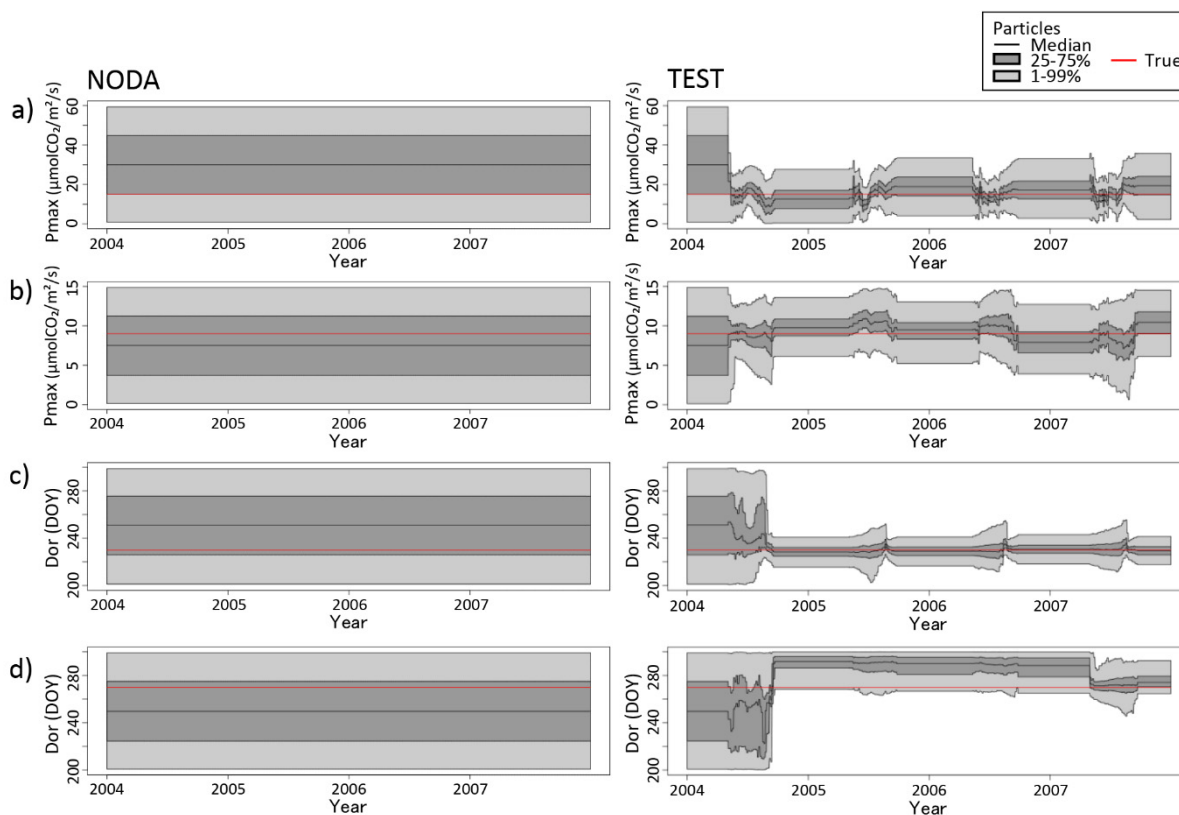


Figure 4. Similar to Fig. 3., but for the model parameters: a) Pmax for forest, b) Pmax for grass, c) Dor for forest, d) Dor for grass. There is no observation for these parameters.

10



5

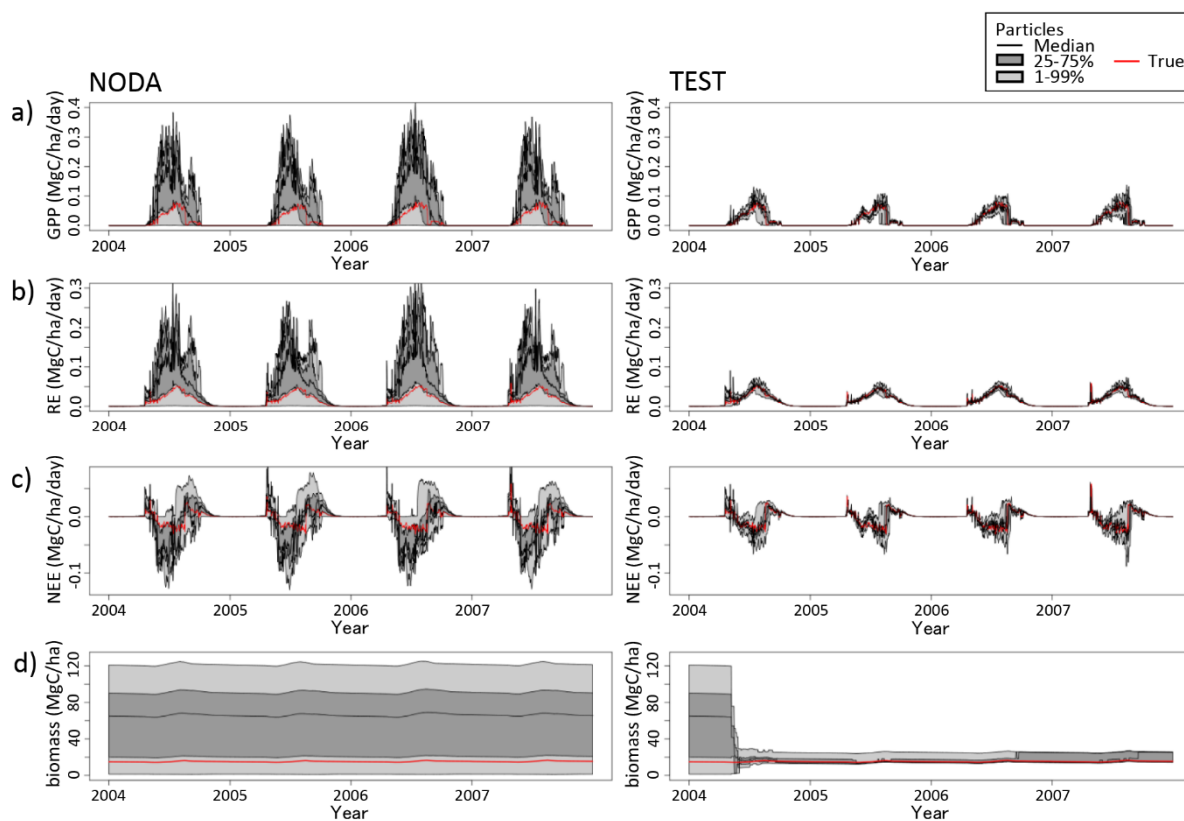


Figure 5. Similar to Figs. 3 and 4, but for unobserved model variables: a) GPP, b) RE, c) NEE, and d) biomass.

10



5

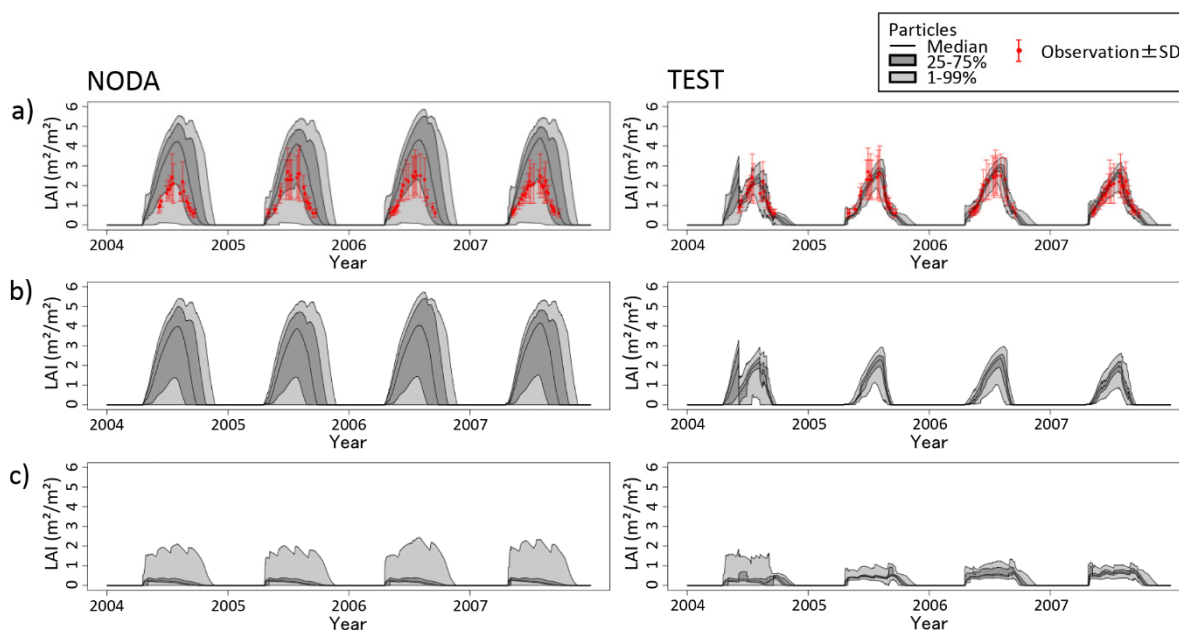
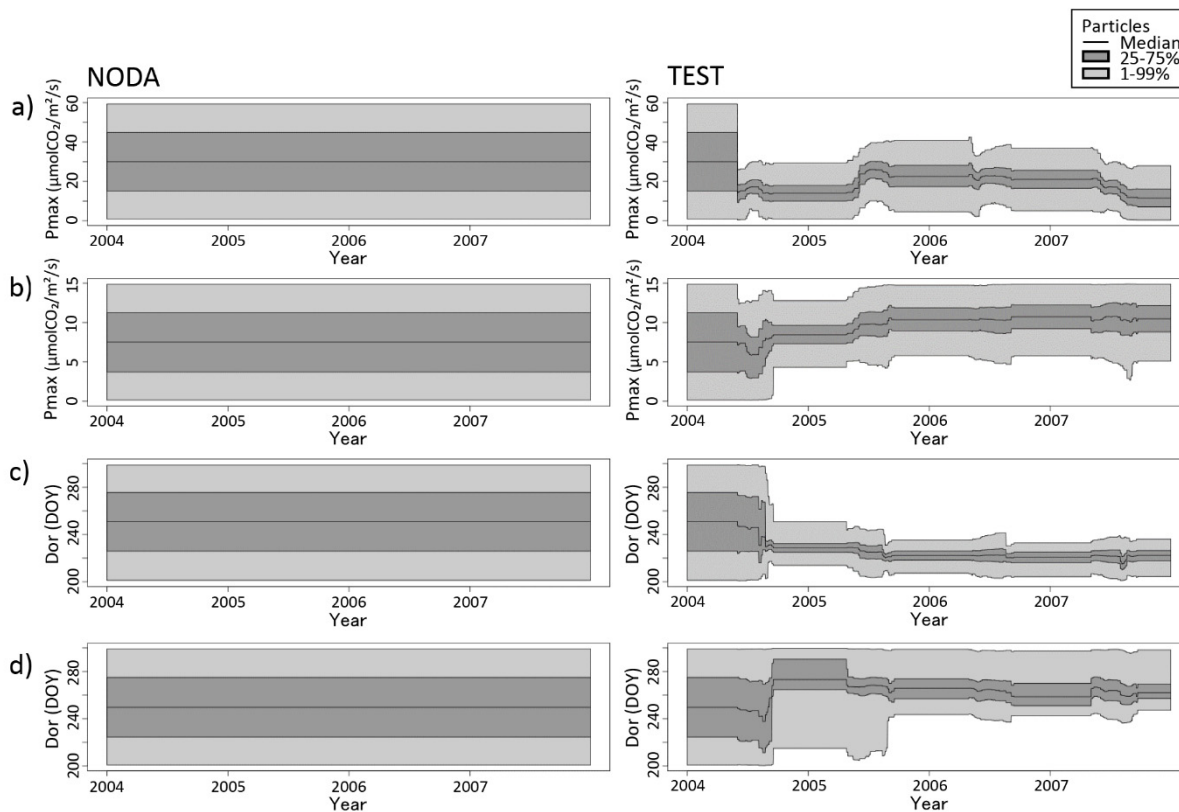


Figure 6. Similar to Fig. 3, showing LAI for a) forest + grass, b) forest, and c) grass, but for the real-world experiment.



5 **Figure 7.** Similar to Fig. 4, showing the model parameters: a) Pmax for forest, b) Pmax for grass, c) Dor for forest, d) Dor for grass, but for the real-world experiment.



5

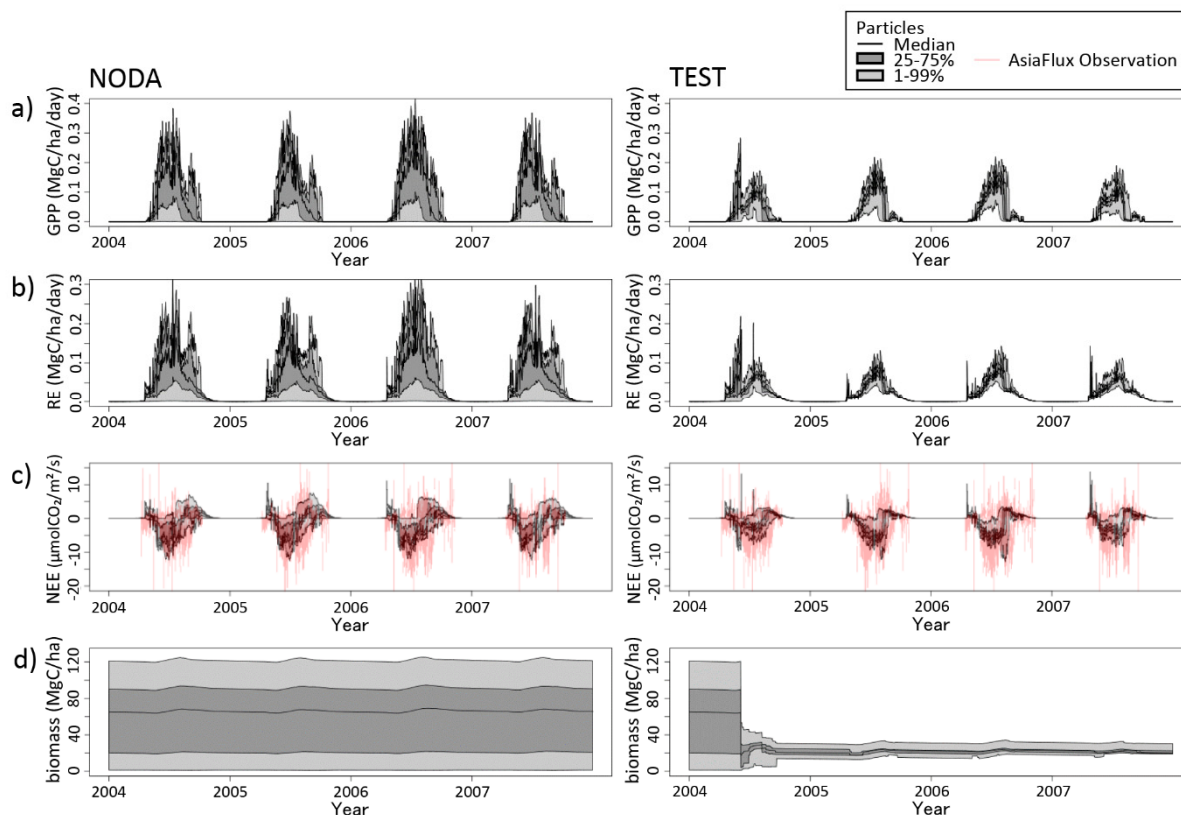


Figure 8. Similar to Fig. 5, showing the unobserved model variables: a) GPP, b) RE, c) NEE, d) biomass, but for the real-world experiment. Red lines indicate the direct field observations made instantaneously every 30 minutes at the AsiaFlux site, while the model simulates only the daily averages.

10